ELSEVIER

Journal of Nuclear Materials 290–293 (2001) 773–777

journal of nuclear materials

www.elsevier.nl/locate/jnucmat

Low-Z impurity transport in DIII-D – observations and implications

M.R. Wade [a,*], W.A. Houlberg [a], L.R. Baylor [a], W.P. West [b], D.R. Baker [b]

[a] *Oak Ridge National Laboratory, Oak Ridge, TN, USA*
[b] *General Atomics, P.O. Box 85608, San Diego, CA 92186-5608, USA*

Abstract

Impurity transport studies on DIII-D have revealed transport phenomena that are qualitatively consistent with that expected from turbulence transport theory in some cases and neoclassical transport theory in other cases. The transport model proposed here, which assumes that the total impurity transport is a linear sum of turbulence-driven transport and neoclassical transport, is shown to reproduce many of these observed features. This transport model is then applied to burn condition calculations, revealing that profile effects associated with neoclassical transport have a large effect on the maximum allowable impurity fraction in machines based on achieving neoclassical transport levels. © 2001 Published by Elsevier Science B.V.

Keywords: Impurity transport; Impurity effects

1. Introduction

The degree to which plasma surface interactions play a critical role in the attainable plasma performance of a reactor-grade fusion plasma is inherently linked to plasma transport of the particles created by such interactions. In particular, the relatively long mean free path of low-Z impurities typically result in ionization sources well away from their generation point at the plasma-surface interface. In such a situation, the inherent transport properties of these impurities in the edge and core plasma become the determining factors in the overall contamination of the core plasma due to these sputtered particles. Therefore, it is crucial to develop an understanding of impurity transport in the edge and core plasmas in order to quantify the maximum level of sputtering yield that is allowed before plasma performance will be adversely affected. On DIII-D, the long-term goal of low-Z core impurity transport studies is to develop a physics understanding of the dominant transport processes in both turbulence-dominated and enhanced confinement plasma regimes, leading to the ability to accurately predict impurity transport in future fusion devices.

In both the SOL and core plasmas, analysis of experimental data suggests that the total impurity transport rate results from a balance between collisional and turbulence-driven transport. This description is based on the premise that the total impurity transport rate is simply a linear combination of collisional (i.e., neoclassical) transport and turbulence-driven transport. This model describes many observations in DIII-D and other tokamaks including: (1) the robust similarity between helium and electron density profiles in all confinement regimes; (2) similarity between low-Z impurity and energy transport rates in turbulence-dominated plasmas; (3) moderately hollow carbon density profiles in H-mode plasmas even when the measured diffusivity is much larger than neoclassical predictions; (4) strongly hollow low-Z density profiles in VH-mode plasmas; and (5) strong accumulation of low-Z impurities in negative central shear (NCS) plasmas with an internal transport barrier (ITB). The ramifications of this theoretical description are far reaching in terms of reactor design and, in some cases, place severe restrictions on the impurity

* Corresponding author. Tel.: +1-858 455 4165; fax: +1-858 455 3492.
E-mail address: wade@alf2.gat.com (M.R. Wade).

0022-3115/01/$ - see front matter © 2001 Published by Elsevier Science B.V.
PII: S0022-3115(00)00499-2

source emanating from the edge plasma. To study this more thoroughly, an ignition calculation similar to those in [1], except with profile effects included, has been carried out to assess the impact of this theory on obtaining ignition in certain confinement regimes. The effect is found to be quite severe in plasmas that exhibit ITBs with the maximum allowable volume-averaged low-Z impurities densities reduced by a factor of 2–5 (depending on the impurity) from the levels allowed with no profile effects included.

A brief description of the theoretical model that is being used as well as the justification for this theory using transport data from DIII-D will be presented in Sections 2 and 3. A brief description of the ignition calculation as well as a sample of the results is presented in Section 3.

2. Impurity transport model

The proposed transport model is based on the premise that particle transport due to fluctuations results from collective mechanisms that have characteristic structures much larger than the characteristic scale length for collisional momentum exchange between particles. This argument, first put forth by Fussman [2], allows one to express the total impurity flux as a simple linear combination of the turbulence-driven and collision-driven (i.e, neoclassical) transport given by

$$\Gamma_Z = -\langle(\nabla_\rho)^2\rangle(D_Z^{\text{turb}} + D_Z^{\text{neoc}})\nabla n_Z + \langle|(\nabla_\rho)|\rangle n_Z(V_Z^{\text{turb}} + V_Z^{\text{neoc}}).$$

Here, $\nabla\rho$ is a geometric factor, D_Z^{neoc} and V_Z^{neoc} are the neoclassical diffusivity and convective velocity, and D_Z^{turb} and V_Z^{turb} are the turbulence-driven diffusivity and convective velocity. The model described here assumes further that $D_Z^{\text{turb}} = D_e^{\text{turb}}$; $V_Z^{\text{turb}} = V_e^{\text{turb}}$. The assumed correspondence between the turbulent impurity and electron transport coefficients is based on the assumption that turbulence-driven transport is dominated by electrostatic turbulence. Since the turbulent-driven particle flux in this case is due to the $E \times B$ drift associated with the fluctuating electric field, particle transport rates should be comparable for all particle species regardless of charge or mass.

To close this set of equations, expressions for D_e^{turb} and V_e^{turb} are required. For comparisons between the theory and experiment, we will use $D_e^{\text{turb}} = \chi_{\text{eff}}^{\text{meas}}$ and $V_e^{\text{turb}}/D_e^{\text{turb}} = (\nabla n_e/n_e)^{\text{meas}}$, where $\chi_{\text{eff}}^{\text{meas}}$ and $(\nabla n_e/n_e)^{\text{meas}}$ are the experimentally measured single-fluid thermal diffusivity and inverse electron density scale length, respectively. These choices are motivated by the usual observation on DIII-D and other tokamaks that electron transport is dominated by anomalous processes (i.e., the electron diffusivities are much larger than neoclassical predictions) [3]. The second assumption is valid if the electron density profile in the core region is not strongly influenced by neutral beam fueling (i.e., $\nabla n_e/n_e > (S_e - dN_e/dt)/n_e D_e^{\text{turb}} A$, where S_e is the volume-integrated electron source rate from neutral beam fueling, N_e the volume-integrated electron density, and A is the surface area at the flux surface of interest). Transport analysis indicates that this provision is met in the cases studied here.

To first order, neoclassical theory predicts that $V_Z^{\text{neoc}}/D_Z^{\text{neoc}}$ to be strongly dependent on the ion density gradient and weakly dependent on the ion temperature gradient: $V_Z^{\text{neoc}}/D_Z^{\text{neoc}} = g_{n_{D\to Z}}\nabla n_Z/n_Z + g_{T_i}\nabla T_i/T_i$, where $g_{n_{D\to Z}} \gg g_{T_i}$. In most plasmas, diffusive transport will be dominated by turbulence-driven transport due to the relative ineffectiveness of collisions in driving cross-field particle transport. However, because of the relatively strong dependence of $V_Z^{\text{neoc}}/D_Z^{\text{neoc}}$ on the plasma profiles, impurity convection can be dominated by neoclassical convection in certain circumstances. Thus, it is possible to observe effects of neoclassical transport even in plasmas in which D_Z^{turb} is significantly larger than D_Z^{neoc} and also to have impurity density profiles that are significantly different from the profile expected purely from turbulence-driven transport or purely from neoclassical transport.

3. Comparison with experiment

The basic features of this transport description are consistent with DIII-D data obtained in a variety of confinement regimes. For example, in highly turbulent plasmas such as L-mode and H-mode, the electron and low-Z (helium, carbon and neon) density profile shapes are approximately the same [4–6], implying that $V_Z/D_Z \sim V_e/D_e$ in these regimes. Also, it is generally found that $D_{e,Z}^{\text{turb}} = \chi_{\text{eff}}^{\text{meas}}$, indicating a strong link between particle and energy transport in these regimes [6–8]. Separate particle transport studies have confirmed the dominance of turbulence-driven particle transport in these plasmas. In particular, non-dimensional scaling studies have shown electron [9] and helium transport [4] to scale proportional with the plasma gyroradius, indicating that small-scale turbulence is the primary transport agent in these plasmas. Other studies have shown that helium transport is very sensitive to the plasma electron temperature with $D_{He} \propto T_e^3$ [10]. Since electron-impurity coupling is weak, neoclassical transport theory predicts very little dependence of D_{He} on T_e.

In contrast, there are distinct differences in the measured density profiles in plasmas that have reduced turbulence. This is most clearly seen in discharges which have distinct ITBs found in DIII-D discharges with NCS and an L-mode edge. In these discharges, an ITB forms in the inner region of the plasma, characterized by

measured ion thermal diffusivities that are essentially zero within the error bars. This low level of transport is observed coincident with a substantial reduction in electrostatic fluctuations, indicating that the turbulent-driven transport has been reduced to small levels. Due to this reduced transport, strong gradients form in both the electron density and ion temperature profiles as shown in Fig. 1(a). The helium density profile is found to have a similar shape as the electron density profile, but strong impurity accumulation on-axis is observed for carbon and neon (Fig. 1(c)). This is qualitatively consistent with neoclassical theory, which predicts impurity accumulation in the presence of a strong main ion density gradient (i.e., $\nabla n_Z/n_Z = g_{n_{D\to Z}}\nabla n_D/n_D$). In VH-mode plasmas in DIII-D, the electron density profile is nearly flat while a strong ion temperature gradient forms in the plasma center as shown in Fig. 1(b). Again, the electron and helium density profile are observed to be similar, but the measured carbon and neon density profiles are significantly more hollow (Fig. 1(d)). Studies [11] have shown that these hollow profiles result from screening of the impurities by a strong ion temperature gradient in the presence of a weak ion density (i.e., $\nabla n_Z/n_z = g_{T_i}\nabla T_i/T_i$, where $g_{T_i} < 0$).

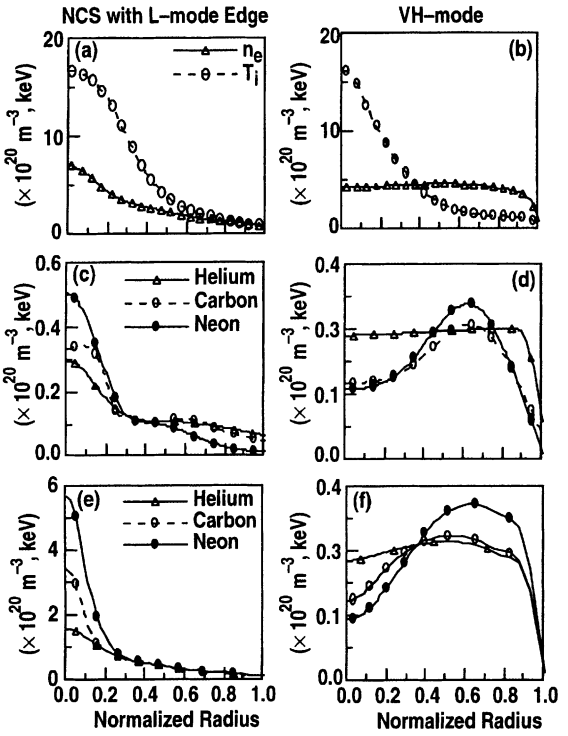

Fig. 1. (a)–(b) Measured electron density and ion temperature profiles, (c)–(d) measured helium, carbon, and neon density profiles (normalized), and (e)–(f) computed helium, carbon, and neon density profiles using the transport model in an NCS and VH-mode discharge in DIII-D.

It is important to note that while qualitative agreement between the features predicted by neoclassical theory and the measured profiles are observed, direct comparisons between the measured transport coefficients and neoclassical theory do not generally give good quantitative agreement – the main discrepancy being between the measured and predicted diffusivities. An example for different light impurities in a VH-mode plasma is given in Fig. 2(a)–(d) [9]. This example shows that while the measured convective velocities are consistent with the neoclassical prediction, the measured diffusivity is substantially larger than the predicted diffusivity. This is believed to be due to the effect of turbulence-driven transport on the measured transport coefficients since the addition of turbulence-driven transport would cause an increase in the effective diffusivity without changing the convective velocity significantly. The diffusivity and convective velocity derived using the model described above are shown in Fig. 2(e)–(f). In this case, good agreement is found between the model's transport coefficients and the measured ones. Further evidence for the validity of this model is provided by comparing the measured density profiles with those computed via the model in the extreme cases of the VH-mode and NCS L-mode discharge profiles. These comparisons are shown in Fig. 1(e)–(f). The model reproduces several key aspects of the measured data. In particular, the helium density profile is predicted to be nearly the same as the electron density profile in both cases – consistent with the measured data. In the NCS case, impurity accumulation on axis is predicted while in the VH-mode case, hollow profiles are predicted – both consistent with the measured data. Finally, the strong Z dependence of the measured profiles is reproduced. For reference, if one assumed that only turbulence-driven transport were present in these cases, all of the impurity density profiles would be similar to the electron density profile. In contrast, if only the neoclassical contribution to the transport were included, the carbon and neon density profiles would be substantially more peaked than the measured profiles in the NCS L-mode case and substantially more hollow than the measured profiles in the VH-mode case.

4. Implications and discussion

The ramifications of this transport model are far reaching in terms of future reactor design, especially considering the present emphasis on improving plasma confinement through turbulence-reduction techniques. Although turbulence reduction is favorable from an energy confinement point-of-view, it can have deleterious effects on overall plasma performance due to unfavorable particle transport characteristics inherent in neoclassical theory. This is especially true in plasmas

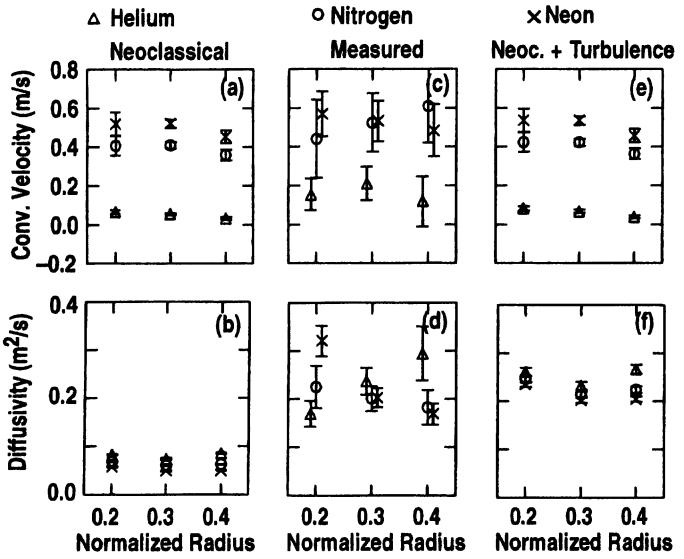

Fig. 2. (a)–(b) Neoclassical predictions, (c)–(d) experimental measurements, and (e)–(f) predictions combining neoclassical and turbulence-driven contributions for a VH-mode discharge in DIII-D [9].

with peaked density profiles in which strong accumulation of low-Z impurities is predicted by neoclassical theory. To study the severity of these effects on plasma performance, a set of burn condition calculations using the impurity transport model described above have been done. The basic equations used in these calculations are the same as those used in [1] with the addition of profile effects through the inclusion of density and temperature profiles. The electron density and temperature profiles are specified and it is assumed that $T_e = T_i = T_z$. The impurity density profile is then calculated self-consistently using the NCLASS code [12] for D_Z^{neoc} and V_Z^{neoc} and assuming $V_Z^{turb}/D_Z^{turb} = (\nabla n_e/n_e)$ and $D_Z^{turb} = \xi D_i^{neoc}$, where ξ is user specified and represents the relative magnitude of turbulent versus collision-driven transport. Note that the inclusion of profiles requires that the obtained solution be self-sustaining (i.e., $P_\alpha > P_{rad}$) across the entire profile. The sustained burn condition (i.e., ignition) is uniquely determined by specification of the temperature profile, τ^*_{He}/τ_E, and the level of impurity contamination. Here, τ^*_{He}/τ_E is the ratio of the global helium confinement to the global energy confinement. The maximum allowable impurity contamination by other impurities is very sensitive to the choice of τ^*_{He}/τ_E. For this calculation, an optimistic value for $\tau^*_{He}/\tau_E = 5$ was chosen to maximize the allowable impurity contamination. Hence, the results can be viewed as an absolute upper limit on the impurity contamination.

To assess the effect of profiles on the burn condition, the density profile is varied while holding the temperature profile fixed. The density profile used is of the form $n_e = n_{e0}(1 - \rho^{1/\alpha})^2$, where α determines the profile peakedness. The maximum allowable volume-averaged carbon and argon fractions f_{max} for several values of ξ are plotted against the profile peaking factor α in Fig. 3. $\xi = 0$ assumes neoclassical transport only, $\xi = 1$ assumes equal contributions of neoclassical and turbulence transport, and $\xi = 100$ assumes turbulence transport only. Note that the case with $\xi = 100$ is essentially equivalent to choosing a flat impurity concentration profile and thus this case serves as a benchmark on the effects of impurity concentration profile. The input and calculated profiles for this reference case ($\xi = 100$) and the extreme cases ($\alpha = 1$ and $\alpha = 0.025$ with $\xi = 0$) are shown for reference in Fig. 4. In the $\alpha = 1$ case, the calculated impurity density profiles are found to be peaked on axis (albeit not as strongly as that shown in Fig. 1(a)). In the $\alpha = 0.025$ case, the impurity profiles are strongly hollow due to temperature screening. In the neoclassical limit (i.e., $\xi = 0$) f_{max} is found to decrease strongly as α increases. In the peaked profile case ($\alpha = 1$), the carbon and neon fractions are limited to ~3.2% and 0.03%, respectively. In contrast, in the flat profile case ($\alpha = 40$), the maximum levels of carbon and neon increase to 7.0% and 0.8 %, respectively. Note that the effect of density profile shape is reduced substantially as the level of turbulence (i.e., ξ) increases. With $\xi = 100$, the maximum allowable impurity fraction f_{max} is found to be weakly dependent on α with f_{max} for carbon and argon – 4.7% and 0.7%, respectively. However, even with equal levels of turbulence-driven and neoclassical transport (i.e., $\xi = 1$, f_{max} is still quite sensitive to α with f_{max} for argon ranging from 0.1% with $\alpha = 1$–0.7% with $\alpha = 0.025$. It is interesting to note that

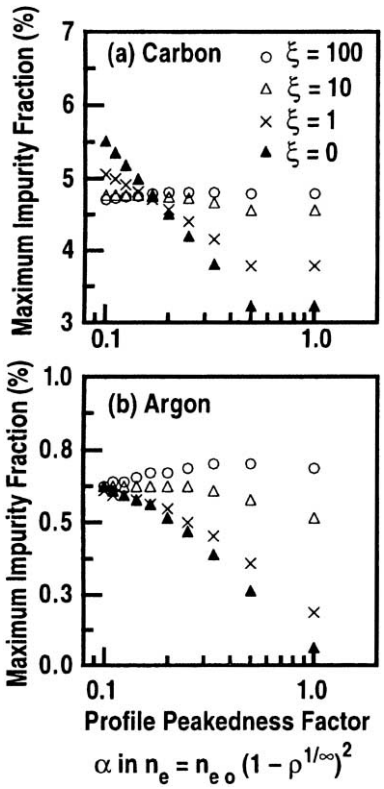

Fig. 3. Maximum allowable volume-averaged density fraction for (a) carbon and (b) argon versus the density profile peakedness factor α for various values $\xi = D_Z^{turb}/D_i^{neoc}$.

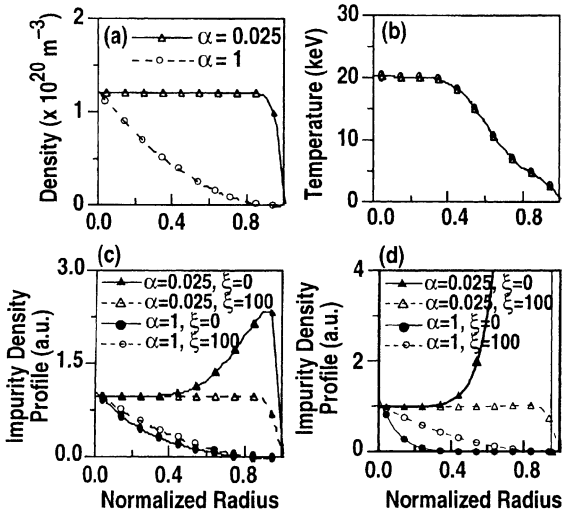

Fig. 4. Input profiles of (a) electron density, (b) temperature, (c) carbon density, and (d) argon density used for various cases in Fig. 3.

the hollow profiles afforded by the temperature screening process with $\alpha \ll 1$ and $\xi < 1$ allow a substantial increase in f_{max} relative to the reference case for carbon. However, such an increase is not seen for argon. This is due to the fact that the limiting factor in the carbon case is fuel dilution while in the argon case the limiting factor is radiation losses.

These results underscore the deleterious effects caused by neoclassical impurity transport when dealing with peaked background density profiles, which are favored from a fusion reactivity standpoint. Fig. 3 however, suggest a different approach – the use of a flat density profile and peaked temperature profile that, in turn, lead to a hollow impurity density profile through the temperature screening process. Such a hollow impurity density profile would have the further benefit of concentrating impurities near the edge of the plasma where efficient radiation can occur while maintaining acceptable fuel dilution in the region of high fusion reactivity. The benefit of the temperature screening process can be obtained even in situations in which turbulent transport dominates the total transport rate. For example, application of this model to the ITER profiles produces hollow carbon and argon density profiles with no discernible effect on the helium profile even when the total transport rate is five times larger than neoclassical predictions.

Acknowledgements

Work supported by the US Department of Energy under Contract Nos. DE-AC03-99ER54463 and DE-AC05-00OR22725.

References

[1] D. Reiter et al., Nucl. Fus. 30 (1990) 2141.
[2] G. Fussman, Plasma Phys. Control. Fus. 33 (1991) 1677.
[3] B. Stallard et al., Phys. Plasmas 6 (1999) 1978.
[4] M.R. Wade et al., Phys. Rev. Lett. 79 (1997) 419.
[5] M.R. Wade et al., in: Proceedings of the 23rd EPS Conference on Controlled Fusion and Plasma Physics, Kiev, Ukraine, vol. 283, European Physical Society, Part I, 1996.
[6] G.M. Staebler et al., Phys. Rev. Lett. 82 (1999) 1692.
[7] M.R. Wade et al., Phys. Plasmas 2 (1995) 2357.
[8] D.R. Baker et al., Nucl. Fus. 40 (2000) 1003.
[9] D.R. Baker et al., Nucl. Fus. 40 (2000) 799.
[10] C.C. Petty et al., Phys. Rev. Lett. 83 (1999) 3661.
[11] M.R. Wade, W.A. Houlberg, L.R. Baylor, Phys. Rev. Lett 84 (2000) 282.
[12] W.A. Houlberg et al., Phys. Plasmas 4 (1997) 3230.